

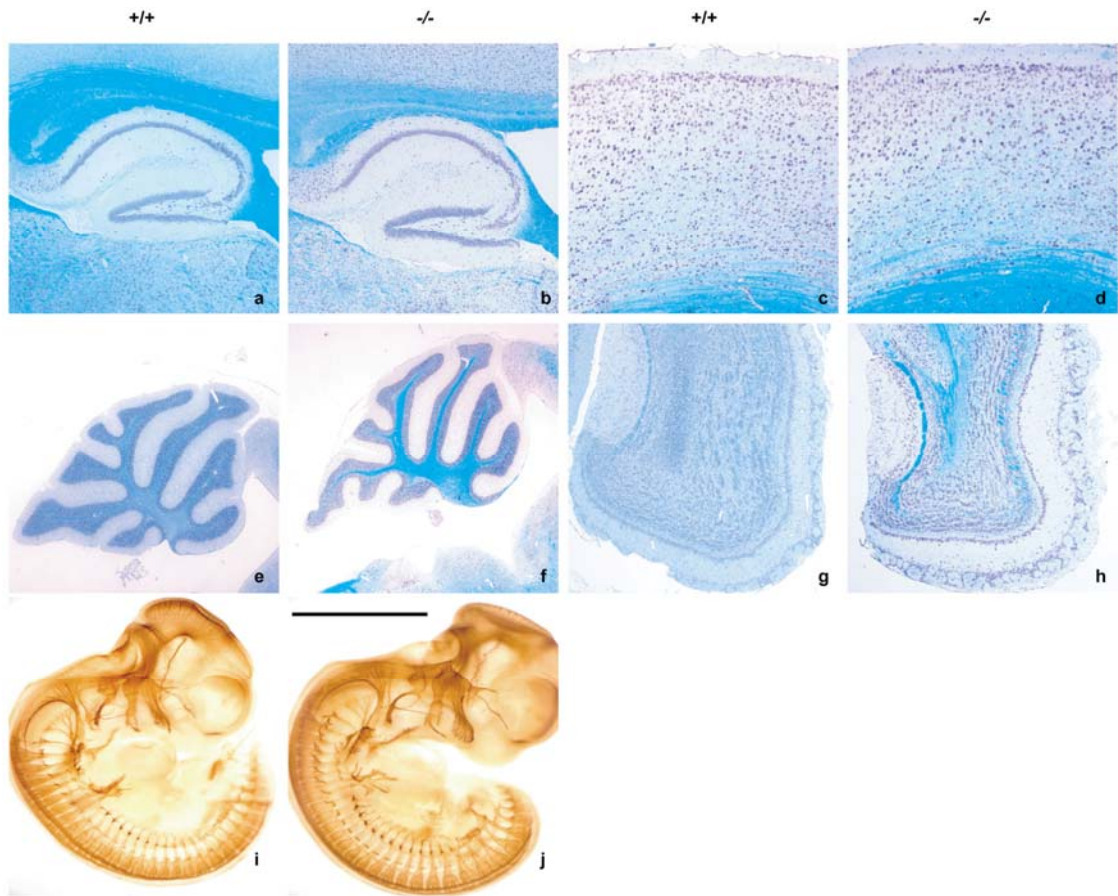
**Supplemental data:**

**Supplemental Figure 1. Sequence of *Dscam* mutation.** Sequencing *Dscam* in cDNA prepared from an affected mouse identified a 38 base pair deletion (arrows) in the sequence encoded by exon 17. The deletion introduces a frame shift, which terminates in a stop codon after 10 amino acids. The deletion was confirmed in genomic DNA. A wild type sequencing chromatogram is shown above that of the mutant. The site of the deletion is marked with arrows. The amino acid translation is shown in the lower right.

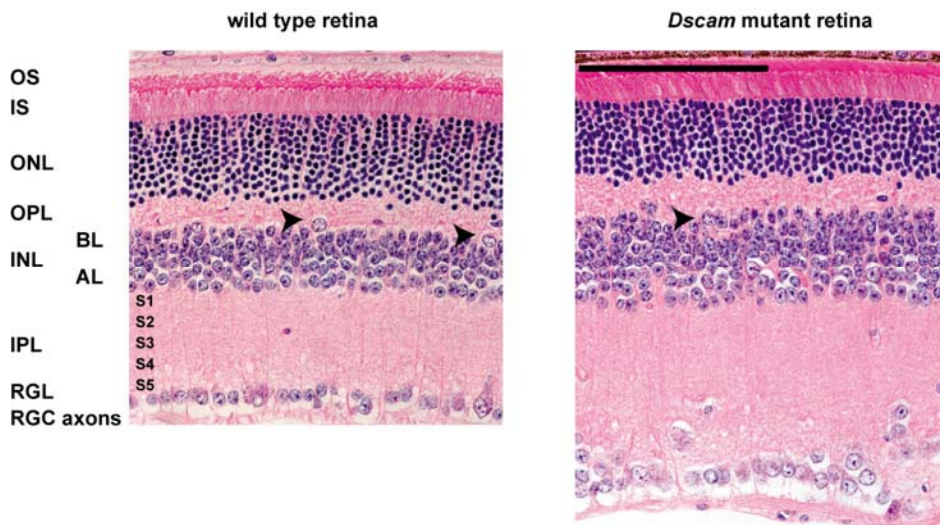


**Supplemental Figure 2. Analysis of *Dscam*<sup>-/-</sup> and wild type nervous system anatomy.**

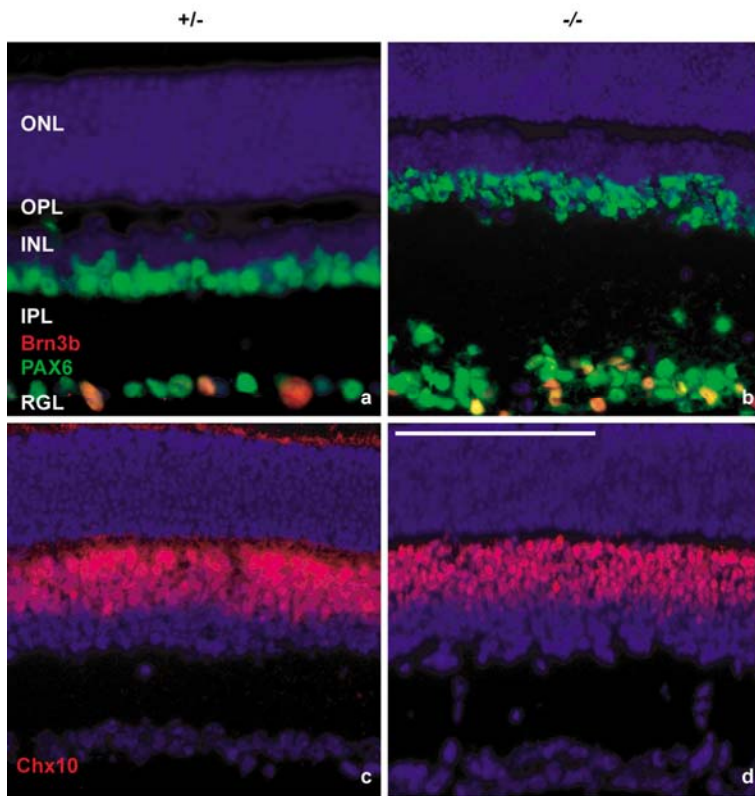
Cresyl violet and luxol fast blue stained coronal sections of control and *Dscam*<sup>-/-</sup> adult brain did not reveal any gross anatomical differences. Laminated CNS structures such as the hippocampus (**a,b**), cerebral cortex (**c,d**), cerebellum (**e,f**), and olfactory bulb (**g,h**) did not show displaced cell bodies or obvious changes in cell density in the mutant mice (**b,d,f,h**). In the cerebellum, the distal portion of the caudal folia were sometimes abnormally long, with thinning of the molecular layer (**f**). The cortical images are from matched rostral/caudal location immediately dorsal to the hippocampal sections shown. The early development of the nervous system, including the peripheral nervous system, was also grossly normal. Embryos were stained using the 2H3 antibody to neurofilament (**i,j**). No difference was observed in the outgrowth of axons in *Dscam*<sup>-/-</sup> embryos compared to controls. Subtle differences that affect specific cell types or specific regions of the CNS could have been overlooked in either of these analyses, and the overt phenotype of the mutant mice indicates that defects beyond the retina are present. The scale bar is equivalent to 900  $\mu\text{m}$  for **a,b**; 505  $\mu\text{m}$  for **c,d**; 2 mm for **e,f**; 1.1 mm for **g,h**; and 700  $\mu\text{m}$  for **i,j**.



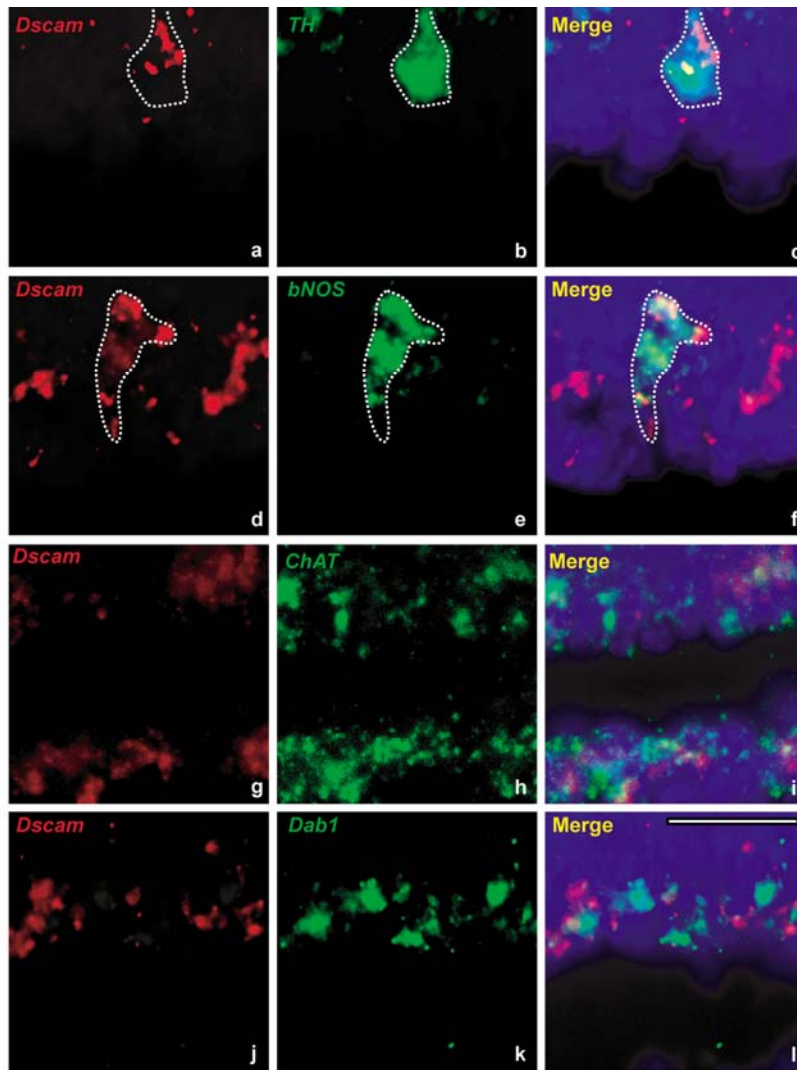
**Supplemental Figure 3. Organization of the wild type and *Dscam*<sup>-/-</sup> retina.** The mouse retina is composed of three nuclear layers and four layers consisting of cellular processes. The photoreceptors of the retina consist of an outer segment (OS) and inner segment (IS). The outer nuclear layer (ONL) contains the nuclei of both rod and cone photoreceptors. The outer plexiform layer (OPL) contains the neurites of horizontal cells and their soma (arrowheads). The inner nuclear layer (INL) is composed of an outer layer of bipolar cells (BL) and an inner layer of amacrine cells (AL). The inner plexiform layer (IPL) consists of the neurites of bipolar, amacrine and ganglion cells. The neurites of different cell population synapse in distinct layers running horizontally through the IPL, which can be subdivided into five strata (S1-S5). The retinal ganglion layer (RGL) consists of a mixture of amacrine cells and retinal ganglion cells. The axons of retinal ganglion cells project to the optic disk and out of the eye. No difference was observed comparing wild type and *Dscam*<sup>-/-</sup> photoreceptors, ONL, OPL or bipolar portion of the inner nuclear layer. There is an increase in the number of amacrine and ganglion cells in the INL and RGL and an increase in the thickness and cellularity of the IPL in the *Dscam*<sup>-/-</sup> retina compared to wild type. The scale bar represents 103  $\mu\text{m}$ .



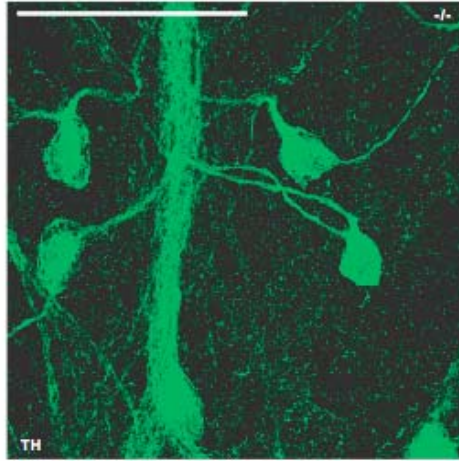
**Supplemental Figure 4. Identification of disorganized cells in the retinal ganglion and inner nuclear layers of the *Dscam*<sup>-/-</sup> retina.** Immunocytochemistry of P10 wild type and *Dscam*<sup>-/-</sup> retina was performed to identify disorganized cell populations. **a,b**, The disorganized cells in the *Dscam*<sup>-/-</sup> inner nuclear layer (INL), inner plexiform layer (IPL) and retinal ganglion layer (RGL) were identified with antibodies against PAX6, a marker of amacrine and ganglion cells, and BRN3b, a marker of a subset of ganglion cells. **c,d**, Immunostaining with antibodies against CHX10, a marker of bipolar cells, was similar in wild type and *Dscam*<sup>-/-</sup> retinas. The scale bar in **d** is equivalent to 120  $\mu\text{m}$  in **a**, 220  $\mu\text{m}$  in **b**, 200  $\mu\text{m}$  in **c,d**. ONL = outer nuclear layer, OPL = outer plexiform layer.



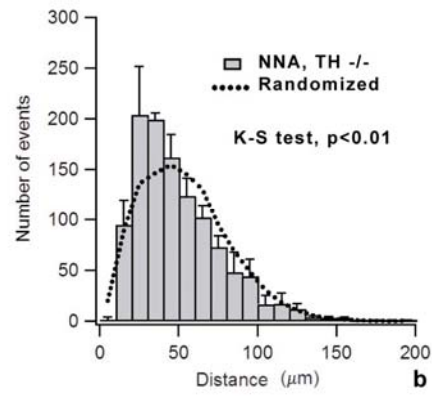
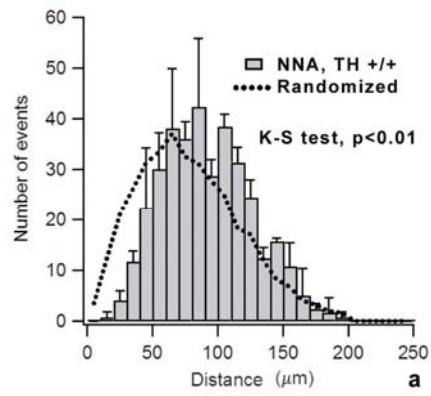
**Supplementary Figure 5. *Dscam* expression in distinct populations of retinal neurons.** *Dscam* expression was assessed in different amacrine cell subtypes using double-in situ hybridization of *Dscam* and amacrine subtype-specific probes. **a-c**, *Dscam* antisense probes colocalized with the majority of *TH*-positive amacrine cells (colocalization >70%, N > 50 *TH*-positive cells examined), and **d-f**, with the majority of *bNOS*-positive amacrine cells (colocalization >77%, N > 70 *bNOS*-positive cells). **g-i**, *Dscam* did not significantly colocalize with *ChAT*, a marker of cholinergic amacrine cells (colocalization <10% N > 50, *ChAT*-positive cells), or **j-l**, with *Dab1*, a marker of AII amacrine cells (colocalization <10%, N > 50 *Dab1*-positive cells). The scale bar in **l** is equivalent to 60  $\mu\text{m}$  in **a-f**, 100  $\mu\text{m}$  in **g-i**, and 75  $\mu\text{m}$  in **j-l**.



**Supplemental Figure 6. Fasciculation and clumping of adult dopaminergic amacrine cells.** In the adult retina, the TH-positive processes of dopaminergic amacrine cells were heavily fasciculated. The cell bodies of these neurons were no longer arrayed in an evenly spaced mosaic pattern, but instead associated with the fascicles. Individual DA neurons in the adult resembled those at P6, with 13 of 25 cells examined in the mutant retinas having crossed primary or secondary processes, which was never seen in 25 wild type cells examined. The scale bar is 80.5  $\mu\text{m}$ .

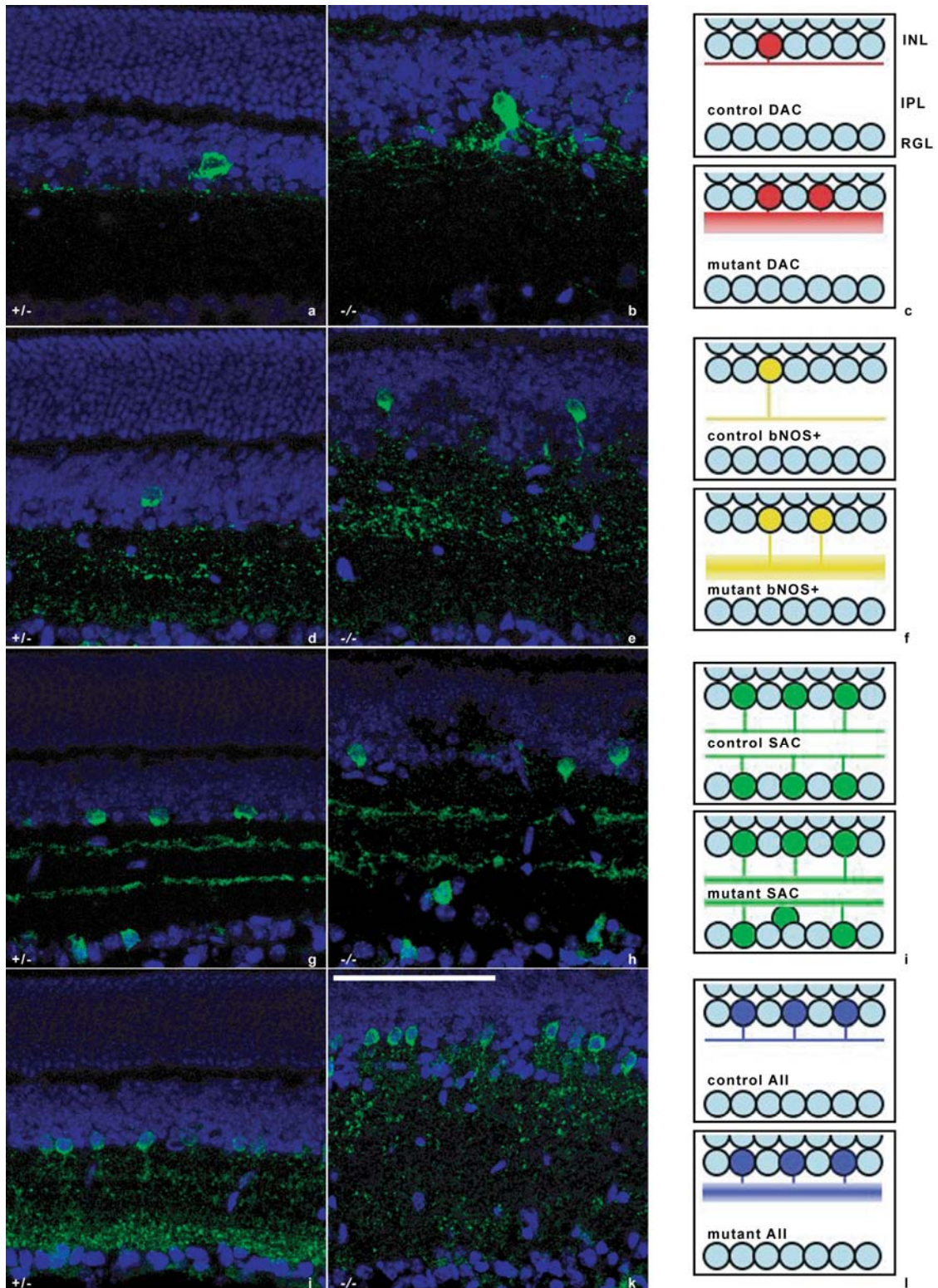


**Supplemental Figure 7. Nearest neighbor analysis (NNA) of dopaminergic amacrine cells.** **a**, NNA of wild type dopaminergic amacrine cells compared to a random simulation indicated the cells are distributed in a statistically significant non-random fashion. A bias for an increased distance between cells compared to the random simulation is indicated by a rightward shift in the distribution. **b**, NNA of *Dscam*<sup>-/-</sup> dopaminergic amacrine cells compared to a random simulation indicated these cells are distributed in a statistically significant non-random fashion, but with a bias for a decreased distance between cells. This is indicated by a leftward shift in the distribution of mutant cells compared to the random distribution. Significance was established using the K-S test and results were  $p < 0.01$  in both cases.

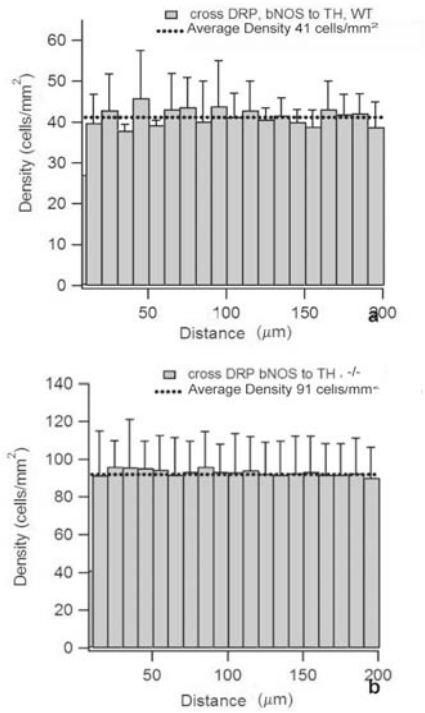


**Supplementary Figure 8. Vertical migration is preserved in the *Dscam*<sup>-/-</sup> retina.**

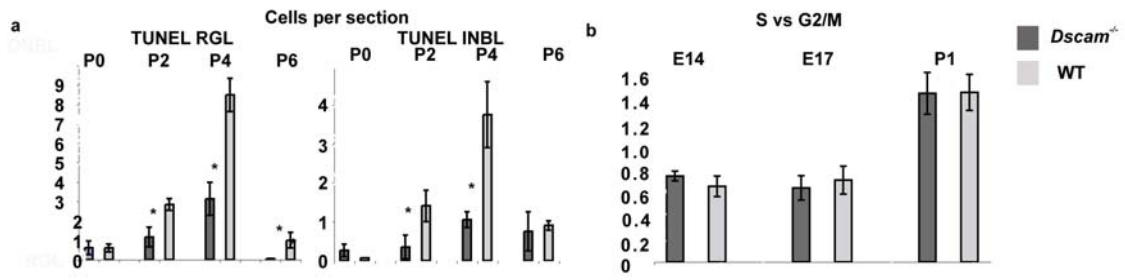
Antibody staining with amacrine cell markers in adult control and *Dscam*<sup>-/-</sup> retinal cross-sections indicated that appropriate cell populations expressed the markers of terminal differentiation, and migrated to the appropriate layer of the retina. Dopaminergic (TH-positive, **a,b**), bNOS-positive (**d,e**), Starburst (ChAT-positive, **g,h**), and AII (DAB1-positive, **j,k**) cells were examined. Schematics **c, f, i** and **l** depict the arborization of wild type and *Dscam*<sup>-/-</sup> neurites in the IPL. In all cell populations, the synaptic laminae in the IPL were broader and less-well defined in the mutant retina than in controls. This is typically more extreme for the cell types that express *Dscam* (dopaminergic and bNOS-positive), though AII, and even ChAT-positive bands showed some disorganization. Given the level of disorganization in the IPL in the *Dscam*<sup>-/-</sup> retina, it is difficult to determine how specific this phenomenon may be. Nuclei were counter stained with DAPI (blue). The scale bar in **k** is equivalent to 150  $\mu\text{m}$ .



**Supplemental Figure 9. Cross-DRP analysis of bNOS- to TH-positive cells.** The reciprocal DRP analysis of bNOS-positive to dopaminergic amacrine cells also indicated that the spacing of these cell populations is independent. No deviations from average cell density were seen at any distance from the reference cell. Taken with the DRPs presented in Figure 4 (TH to bNOS), this indicates that neither population depends on the other.



**Supplemental figure 10. Cell death is decreased in the *Dscam*<sup>-/-</sup> retina, while mitotic index is unchanged.** **a**, Cell death was examined by counting the number of TUNEL positive nuclei in the wild type and *Dscam*<sup>-/-</sup> retina at time points corresponding to normal developmental cell death of retinal ganglion and amacrine cells. A significant decrease in the number of TUNEL-positive cells in the *Dscam*<sup>-/-</sup> retinal ganglion layer was observed at P2, P4 and P6 by TUNEL analysis. A significant decrease in the number of TUNEL-positive cells in the *Dscam*<sup>-/-</sup> retina was also observed in the inner neuroblast layer, which was differentiated from the outerneuroblast layer by PAX6 immunoreactivity, at P2 and P4. **b**, No significant change was observed in the mitotic index of the *Dscam*<sup>-/-</sup> and wild type retina.



**Supplemental figure 11.** Mosaic analysis of dopaminergic amacrine cell lineage. Using an X-linked YFP transgenic strain that expresses in dopaminergic amacrine cells allowed a clonal analysis of aggregated cell bodies by taking advantage of X-inactivation in female mice. **a**, In the rare instances of closely associated DA cells in control mice, the two cells were from different clones (based on the X-inactivation pattern) at approximately random frequencies. **b**, In the clumped TH-positive cell bodies in the *Dscam*<sup>-/-</sup> retinas, the cells were again from different clonal progenitors. The scale bar in **b** represents 107  $\mu\text{m}$  in **a** and **b**.

